Experimental characterization of Inconel 625 powder stream and single track deposited on SS400 steel by direct laser metal deposition

Nguyen Quoc Tuan, Nguyen Van Quan, Doan Tat Khoa,
Duong Quoc Dung, Nguyen Minh Dat, Trinh Quang Hung*

Faculty of Mechanical Engineering, Le Quy Don Technical University, 236 Hoang Quoc Viet, Nghia Do, Hanoi, Vietnam.

*Corresponding author: trinhquanghung@lqdtu.edu.vn

Received 10 Mar. 2026; Revised 4 May 2026; Accepted 11 May 2026; Published 25 Aug. 2026.

DOI: https://doi.org/10.54939/1859-1043.j.mst.113.2026.168-175

ABSTRACT

Directed laser metal deposition (DLMD) offers significant potential for producing high-performance coatings and functional components, yet the effect of powder feed rate on coaxial powder stream stability and its correlation with single-track deposition quality remains insufficiently investigated. This study characterizes the Inconel 625 powder stream using light-sheet imaging and grayscale intensity analysis at feed rates of 5–30 g/min. The powder stream consistently converged at approximately 9 mm below the nozzle exit, independent of feed rate, ensuring stable alignment with the laser beam without adjusting the stand-off distance. The transverse profiles exhibited a Gaussian-like distribution. Based on these findings, single-track deposition on SS400 steel produced stable geometry, a fine cellular-to-columnar dendritic microstructure (primary dendrite arm spacing of 2.2–2.3 µm), uniform microhardness of 206.7–209.5 HV (about 25% higher than the substrate), and no porosity, lack-of-fusion, or solidification cracks. These results establish a direct link between powder stream characteristics and deposition quality, providing practical guidelines for robust DLMD processing of Inconel 625 on carbon steel substrates.

Keywords: Direct laser metal deposition; Inconel 625; Powder stream characterization; Coaxial nozzle; Single track; Microstructure and microhardness

1. INTRODUCTION

Directed laser metal deposition (DLMD), a directed energy deposition (DED) technique, enables the fabrication of near-net-shape components and high-performance coatings by delivering metallic powder into a laser-induced melt pool [1, 14]. It offers excellent metallurgical bonding, controlled dilution, and the capability to deposit dissimilar materials such as Inconel 625 on carbon steels [2]. Although carbon steels are widely used due to their low cost, their poor corrosion resistance limits service life, particularly in tropical environments with high humidity and chloride exposure [3, 4]. Applying Inconel 625 by DLMD is therefore an effective approach to improve corrosion resistance while maintaining economic efficiency [5,6]. Previous studies have reported fine cellular-to-columnar dendritic microstructures, Nb- and Mo-rich interdendritic Laves phase and MC carbides, and enhanced hardness in DLMD-fabricated Inconel 625 [7].

The powder stream in DLMD is governed by carrier gas flow, nozzle geometry, particle interactions, and powder feed rate [8-10]. Variations in feed rate influence particle concentration, convergence position, stream diameter, and powder distribution, thereby affecting powder catchment efficiency, melt pool stability, and deposition quality. Light-sheet imaging based on Mie scattering theory provides an effective non-contact method for characterizing powder streams through grayscale intensity analysis [11]. Although numerical studies have extensively investigated powder flow [8, 12, 13], experimental studies directly correlating powder stream characteristics with single-track deposition quality remain limited.

In this study, the Inconel 625 powder stream delivered through a coaxial nozzle was experimentally characterized over feed rates of 5–30 g/min using light-sheet imaging and grayscale analysis. The convergence position, particle density, and transverse distribution were quantified, followed by single-track deposition on SS400 steel. The deposited tracks were evaluated in terms of geometry, microstructure, and mechanical properties to determine whether feed-rate variations require stand-off or laser realignment and to establish practical guidelines for stable DLMD processing of Inconel 625 on carbon steel.

2. MATERIALS AND METHODS

2.1. Experimental setup and materials

Experiments were conducted using a DLMD system (Figure 1) comprising a 500 W fiber laser (YLR-500-WC, IPG), a coaxial powder nozzle, a rotating-disk powder feeder, and a multi-axis Computer Numerical Control (CNC) stage. A Gaussian laser beam ($M^2 = 1.1$) was delivered through an optical fiber and focused by a 190 mm focal-length lens. The coaxial nozzle featured four 5 mm powder inlets inclined at 60° and an annular outlet with inner/outer diameters of 10/12 mm. Inconel 625 powder was delivered using nitrogen as both the carrier gas (6 L/min) and shielding gas (8 L/min). SS400 steel substrates (160 × 160 × 8 mm) were ground and solvent-cleaned before deposition. The chemical compositions of the powder and substrate are listed in Table 1 and Table 2.

Table 1. *Chemical composition of Inconel 625 powder.*

%C	%Si	%Mn	%P	%S	%Cr	%Mo
0.03-0.10	≤ 0.5	≤ 0.5	≤ 0.02	≤ 0.015	20-23	8.0-10.0
%Ni	**%Ti**	**%Cu**	**%Al**	**%Co**	**%Fe**	**%Nb**
≥ 58	≤ 0.4	≤ 0.5	≤ 0.4	≤ 1.0	≤ 5.0	3.15-4.15

Table 2. *Chemical composition of SS400 steel.*

%C	%Si	%Mn	%P	%S	%Ni	%Cr	%Fe
0.11-0.18	0.12-0.17	0.4-0.57	≤ 0.05	≤ 0.05	≤ 0.03	≤ 0.02	Bal.

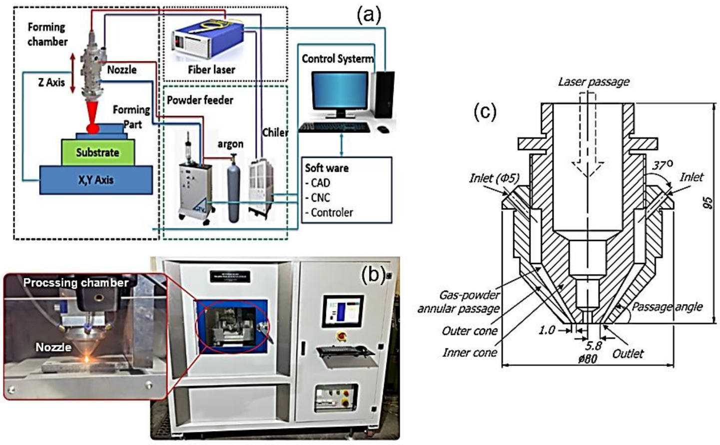

Figure 1. *(a) schematic and (b) actual DLMD system with (c) a coaxial powder nozzle.*

2.2. Powder stream imaging and analysis

Powder stream characteristics were characterized with the processing laser turned off to eliminate thermal radiation interference. A 30 mW, 532 nm green laser and a cylindrical lens generated a thin light sheet for longitudinal (Figure 2a), while transverse imaging used a 45° mirror to reflect the spot into the camera (Figure 2b). Feed rates from 5 to 30 g/min were tested to evaluate particle density and convergence behavior. The actual experimental setup and obtained images are shown in Figure 2c.

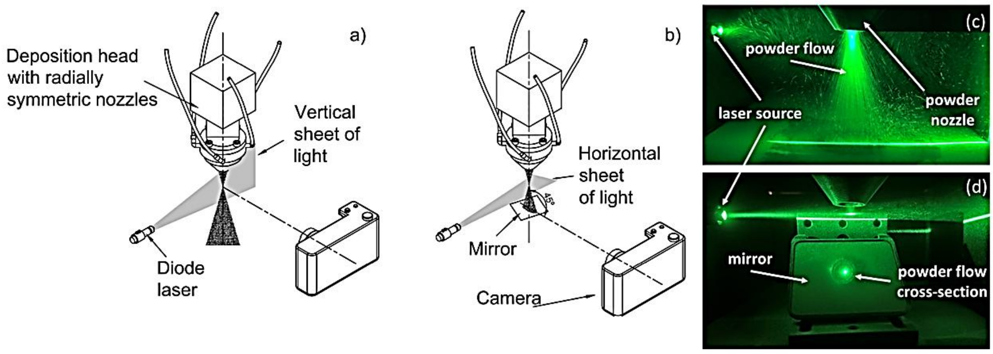

Figure 2. *Experimental setup for imaging the powder stream: (a) and (c) axial cross-sections, (b) and (d) radial cross-sections.*

Captured images were processed using ImageJ (version 1.54g) to extract grayscale intensity profiles along the nozzle centerline and selected transverse sections (Figure 3). Based on Mie scattering theory, grayscale intensity was used as a qualitative indicator of particle concentration and to identify the convergence position and effective stream diameter. Since multiple scattering and signal saturation occur at high feed rates, grayscale intensity was used for relative comparison rather than absolute particle concentration.

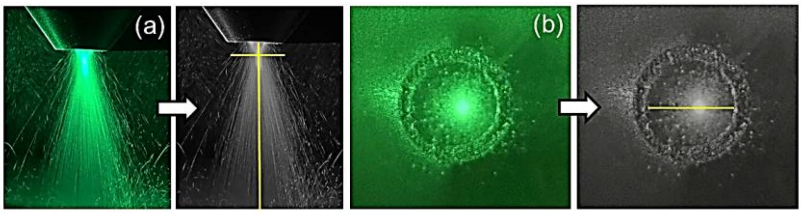

Figure 3. *Image processing of powder stream cross-section using ImageJ: (a) transverse image and (b) longitudinal image.*

2.3. Single-track deposition

To validate the characterized powder stream conditions, a single-track deposition of Inconel 625 on an SS400 steel substrate was performed using a laser power of 450 W, a scanning speed of 300 mm/min, a powder feed rate of 10 g/min, and a stand-off distance of 9 mm, selected based on the powder stream characterization (Section 3.1).

The deposited track was sectioned at mid-length by wire-cut Electrical Discharge Machining (EDM), metallographically prepared, etched with Kalling's No. 2 reagent, and examined by Scanning Electron Microscope (SEM; JSM-IT800, JEOL). Track geometry (width, height, penetration depth, and contact angle) was measured using ImageJ, while dilution was calculated according to Equation (1).

$$Dilution(\%) = \frac{d}{(d+h)} \times 100 \qquad (1)$$

Vickers microhardness testing was carried out across the deposited layer and substrate using a Vickers microhardness tester (Affri DM2D, AFFRI). Measurements were performed with a load of 100 g (HV0.1) applied for 10 seconds.

3. RESULTS AND DISCUSSION

3.1. Powder stream characterization

3.1.1. Longitudinal distribution

Figure 4 shows how the powder stream evolves with feed rate. At 5 g/min the convergence zone is faint, indicating low particle density, while 10 g/min produces a brighter, more concentrated region. The inset in Figure 4b reveals a bright central core with a Gaussian-like distribution, highest at the center and decreasing outward. Beyond 15 g/min, overall brightness saturates and the core elongates axially, a response caused by shielding and multiple scattering in the dense cloud, as well as camera limitations, which restrict the apparent rise in intensity.

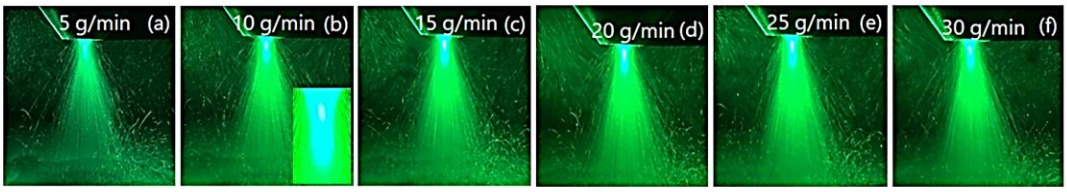

Figure 4. *Longitudinal images of powder stream at different powder feed rates (5 to 30 g/min).*

Figure 5 shows longitudinal intensity profiles along the nozzle axis. For all feed rates, grayscale intensity rises sharply below the nozzle exit, peaks, then gradually decreases, confirming a stable convergence zone. The peak position (approximately 9 mm) remains nearly unchanged, indicating that feed rate does not affect convergence, which is governed by nozzle geometry and carrier gas flow. This invariance means deposition productivity can be adjusted via feed rate without reconfiguring laser focus or stand-off distance.

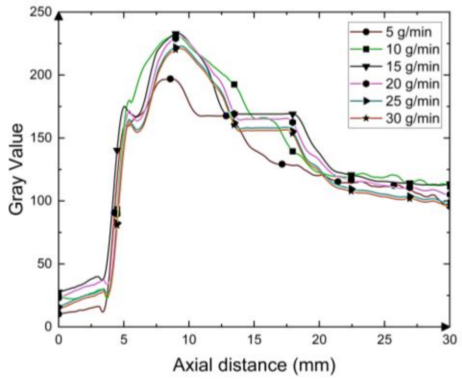

Figure 5. *Longitudinal intensity distributions of the powder stream at different powder feed rates.*

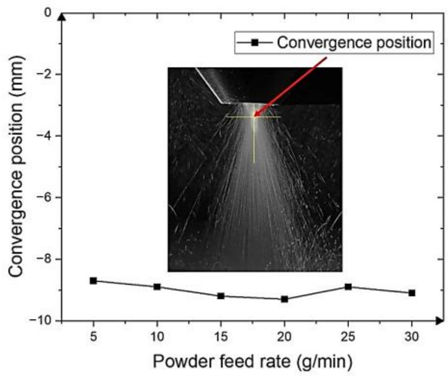

Figure 6. *Convergence position of the powder stream at different powder feed rates.*

In terms of particle density, the peak or maximum intensity increases markedly as the feed rate rises from 5 to 10 g/min, indicating a higher powder concentration within the convergence zone. At feed rates beyond 10 g/min, however, the peak intensity slightly decreases, likely due to the saturation-like response in the captured images. This apparent optical saturation does not imply that particle concentration in the convergence zone ceases to increase.

Figure 6 shows the relationship between feed rate and convergence position. Despite minor fluctuations, the convergence point remains close to -9 mm downstream of the nozzle exit, confirming that feed rate mainly affects particle density rather than shifting the focal position. This stability ensures reliable overlap between the powder focus and laser beam, allowing productivity to be adjusted by feed rate without altering nozzle setup or laser alignment. The result highlights the robustness of the system and simplifies DLMD process control.

3.1.2. Transverse distribution

Figure 7 shows transverse intensity profiles at the convergence positions, extracted along a horizontal line from the longitudinal images (see Figure 3a). These profiles provide an indirect evaluation of the transverse powder distribution based on the projection of particle concentration in the longitudinal plane. All feed rates exhibit a Gaussian-like particle distribution, characterized by a pronounced centerline peak and symmetric radial decay. From 5 to 10 g/min, peak intensity rises and the profile broadens, indicating higher particle density and lateral spreading; changes diminish at higher rates due to saturation. Results at higher powder feed rates (≥ 20 g/min) are not shown because significant gray-level saturation occurs, leading to loss of linearity between image intensity and particle concentration.

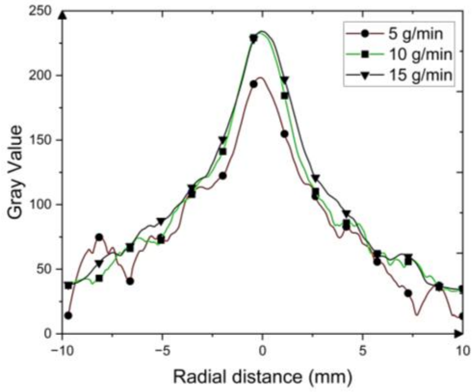

Figure 7. *Transverse intensity at convergence position under different feed rates.*

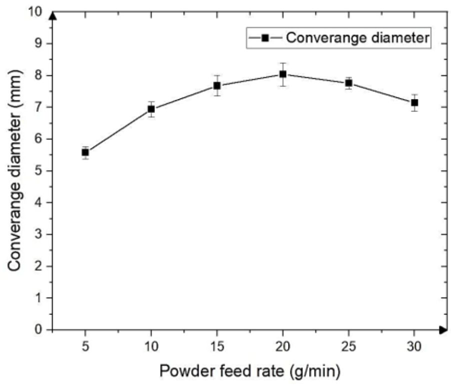

Figure 8. *Convergence diameter under different feed rates.*

Figure 8 shows that the convergence diameter increases steadily from about 5 to 8 mm reflecting higher particle numbers as the feed rate rises from 5 to 20 g/min. At higher feed rates, the apparent reduction remains unclear, though improved imaging could provide more reliable characterization under dense flow. A larger diameter reduces overlap with the laser beam, increasing powder loss, so feed rate must be carefully controlled to avoid excessive broadening.

As shown in Figure 6, the convergence position remains stable at about 9 mm downstream of the nozzle exit, allowing the stand-off distance to be fixed for all feed rates. Figure 9 presents transverse cross-sections at this position up to 15 g/min, where the spots remain nearly round, confirming symmetric particle distribution and nozzle stability. With increasing feed rate, brightness intensifies and the spot gradually enlarges, indicating higher particle density without significantly shifting the convergence position. This stability, as earlier mentioned, enables consistent laser alignment and simplifies DLMD process control. Similar to Figure 7, results at higher powder feed rates (≥20 g/min) are omitted due to gray-level saturation.

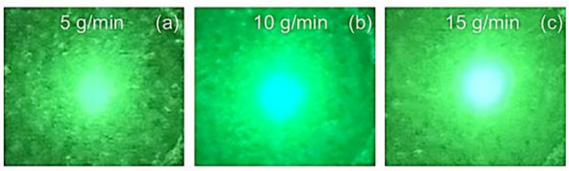

Figure 9. *Transverse cross-sections of the powder stream at -9 mm from the nozzle exit under different powder feed rates.*

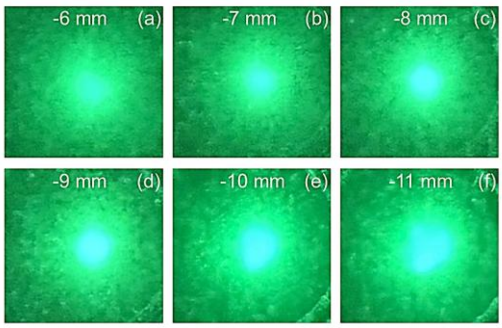

Figure 10. *Transverse cross-sections of the powder stream at different axial positions with a feed rate of 10 g/min.*

To examine powder-flow evolution, transverse cross-sectional images (Figure 10) were recorded at different axial positions below the nozzle exit with a feed rate of 10 g/min. In the near-nozzle region (-6 to -7 mm), the distribution appears diffuse, reflecting lower particle concentration. With increasing distance, the stream brightens and becomes most compact around -8 to -9 mm, before diverging again at -10 to -11 mm. Across all positions, the nearly round cross-sections confirm symmetric particle distribution, supporting uniform clad formation.

The corresponding transverse intensity profiles at different axial positions of the 10 g/min stream are shown in Figure 11. Both the raw curves (Figure 11a) and their smoothed counterparts (Figure 11b) are presented. In Figure 11a, the "0" position corresponds to the maximum intensity in the convergence plane at -9 mm. Despite minor fluctuations caused by measurement noise and stochastic particle behavior, the raw profiles almost share the same central peak at "0" position, demonstrating the high stability of the powder stream. The smoothed curves emphasize the underlying Gaussian-like distribution and symmetry of the stream. Moreover, the peak intensity increases progressively as the imaging plane shifts from -6 mm to -9 mm, before decreasing beyond this point. This behavior clearly confirms the convergence position at approximately -9 mm, in agreement with the longitudinal intensity profiles previously shown in Figure 5.

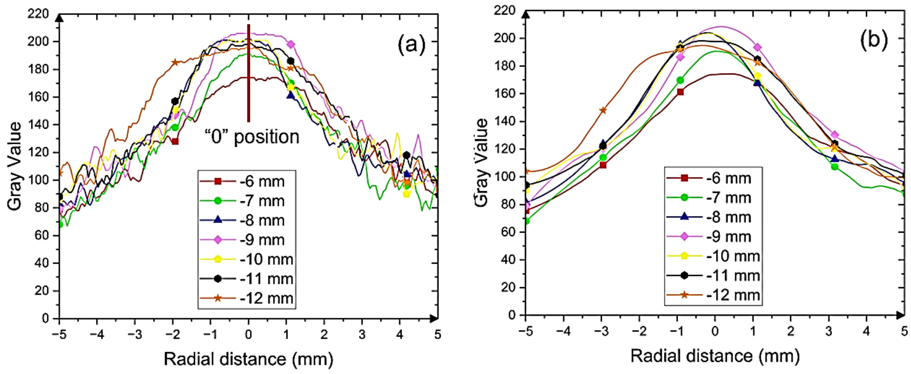

Figure 11. *Gray value profiles of transverse cross-sections at different axial positions with a feed rate of 10 g/min: (a) raw curves without smoothing and (b) smoothed curves.*

3.2. Single-track deposition characteristics

Based on the powder stream characterization (Section 3.1), a stand-off distance of 9 mm was selected for single-track deposition to maximize powder concentration at the melt pool. Figure 12 shows the SEM cross-section of an Inconel 625 track deposited on SS400 at 450 W, 300 mm/min, and 10 g/min. The bead exhibits a nearly symmetric elliptical profile, consistent with the Gaussian powder distribution and laser beam profile, indicating good correlation between powder flow and deposition geometry. The measured width, height, penetration depth, wetting angle, and dilution were 0.96 mm, 0.15 mm, 0.11 mm, 32°, and 42%, respectively.

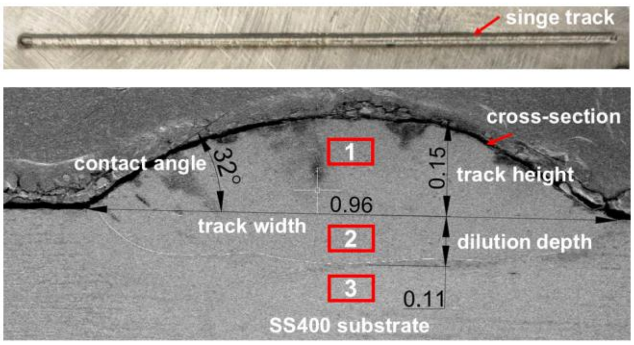

Figure 12. *The deposited single track and its cross-section geometry.*

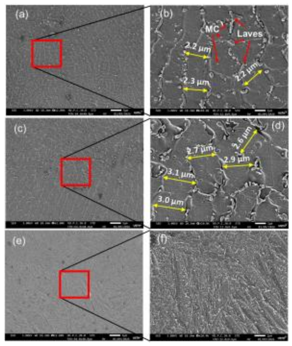

Figure 13. *Microstructure of the single-track cross-section (a-d) and substrate (e-f).*

Microstructural characterization was conducted at multiple locations along the track height. Higher-magnification SEM images of the microstructure in the three representative regions marked in Figure 12 are presented in Figure 13. The microstructure in this region consists of fine cellular-to-columnar dendrites with a primary dendrite arm spacing (PDAS) of approximately 2.2-

2.3 μm. Interdendritic MC-type carbides and Laves phase are observed, indicating Nb and Mo segregation during solidification [7]. Such segregation behavior is widely recognized as a characteristic feature of rapidly solidified Ni-based superalloys.

Figures 13c and 13d show the microstructure in region 2, representing the transition between the clad and the substrate. Compared to the clad region, the dendritic structure here becomes slightly coarser, with PDAS increasing to approximately 2.6-3.1 μm. This coarsening is associated with a reduced cooling rate and compositional mixing between the Inconel 625 and the SS400 substrate. In the lower part of this region, a clear transition in morphology is observed from cellular-like structures to elongated, well-oriented columnar dendrites. This change is attributed to the increasing influence of directional heat extraction toward the substrate, which promotes epitaxial growth. The presence of such columnar structure near the interface indicates strong metallurgical bonding. Figure 13e and 13f illustrate the substrate region, where the original microstructure of SS400 is observed. The microstructure is characterized by a typical ferrite-pearlite structure, without dendritic features. No porosity, lack-of-fusion defects, or cracks were detected across the regions, indicating good metallurgical integrity. However, microsegregation may locally influence mechanical properties and corrosion resistance.

Figure 14 shows the Vickers microhardness profile across the clad. Uniform values of 206.7-209.5 HV were measured within the deposit (locations 1-3), about 25% higher than the substrate hardness (location 4). This increase is attributed to the fine cellular-columnar dendritic microstructure, solid-solution strengthening from Nb, Mo, and Cr in the γ-FCC matrix, and dispersion strengthening from interdendritic phases. The hardness enhancement demonstrates the effectiveness of DLMD in producing functional coatings or features on carbon-steel substrates.

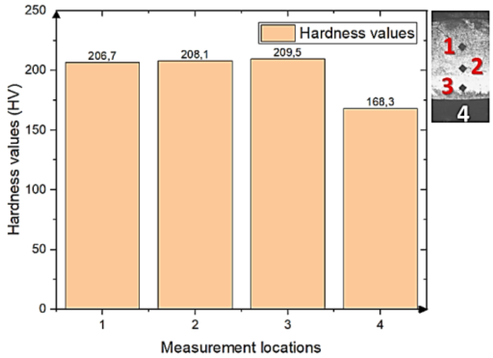

Figure 14. *Microhardness of the deposited single track.*

4. CONCLUSIONS

This study presents a systematic experimental investigation of Inconel 625 powder stream behavior through a coaxial nozzle and its translation into single-track deposition on SS400 steel by direct laser metal deposition. The powder stream convergence position remained stable at approximately 9 mm downstream of the nozzle exit across the entire feed-rate range of 5 to 30 g/min, while particle density and convergence diameter exhibited clear dependence on mass flow rate. Transverse distributions followed a Gaussian-like profile. These characteristics ensured optimal overlap between the powder focus and the laser beam and enabled the selection of a fixed stand-off distance, resulting in a defect-free single-track deposit with columnar dendritic growth, refined PDAS of 2.2-2.3 μm, and homogeneous microhardness enhancement of about 25% relative to the substrate. Future research will extend to optimization of process parameters, multi-layer builds, post-deposition heat treatments to mitigate microsegregation and detailed assessment of long-term corrosion resistance and fatigue behavior.

Acknowledgement: *This research is funded by Le Quy Don Technical University.*

REFERENCES

[1]. G. P. Dinda et al., "*Laser aided direct metal deposition of Inconel 625 superalloy: Microstructural evolution and thermal stability*", Mater. Sci. Eng. A, Vol. 509, pp. 98–104, (2009).

[2]. J. Cheng et al., "*An overview of laser metal deposition for cladding: Defect formation mechanisms, defect suppression methods and performance improvements of laser-cladded layers*", Materials, Vol. 15, No. 16, p. 5522, (2022).

[3]. Tran Van Cuong et al., "*Study on the effect of halloysite nanotubes on the adhesion and corrosion protection of epoxy coatings on carbon steel*", J. Mil. Sci. Technol., No. IMBE, pp. 179–185, (2025).

[4]. Nguyen Van Son et al., "*Investigation of environment parameters and metal corrosion rate n atmospheric enviroment at Phan Thiet*", J. Mil. Sci. Technol., No. 84, pp. 80–85, (2022).

[5]. Y. Ma et al., "*The atmospheric corrosion kinetics of low carbon steel in a tropical marine environment*", Corros. Sci., Vol. 52, pp. 1796–1800, (2010). DOI: 10.1016/j.corsci.2010.01.022.

[6]. R. E. Melchers, "*Long-term corrosion of cast irons and steel in marine and atmospheric environments*", Corros. Sci., Vol. 68, pp. 186–194, (2013). DOI: 10.1016/j.corsci.2012.11.014.

[7]. F. Zafar et al., "*A review on direct laser deposition of Inconel 625 and Inconel 625-based composites-challenges and prospects*", Metals, Vol. 13, No. 4, p. 787, (2023). DOI: 10.3390/met13040787.

[8]. L. Li et al., "*Numerical study on powder stream characteristics of coaxial laser metal deposition nozzle*", Crystals, Vol. 11, No. 3, p. 282, (2021). DOI: 10.3390/cryst11030282.

[9]. X. Guan et al., "*Numerical modeling of coaxial powder stream in laser-powder-based directed energy deposition process*", Addit. Manuf., Vol. 34, p. 101226, (2020). DOI: 10.1016/j.addma.2020.101226.

[10]. K. Wang et al., "*Powder stream performance of a novel annular laser direct metal deposition with inside-laser coaxial powder feeding nozzle: Simulation and experimental perspectives*", Opt. Laser Technol., Vol. 175, p. 110723, (2024). DOI: 10.1016/j.optlastec.2024.110723.

[11]. P. Balu et al., "*Parametric study on a coaxial multi-material powder flow in laser-based powder deposition process*", J. Mater. Process. Technol., Vol. 212, pp. 1598–1610, (2012).

[12]. N. Tamanna et al., "*Progress in numerical simulation of the laser cladding process*", Opt. Lasers Eng., Vol. 122, pp. 151–163, (2019). DOI: 10.1016/j.optlaseng.2019.05.026.

[13]. J. Lin, "*Numerical simulation of the focused powder streams in coaxial laser cladding*", J. Mater. Process. Technol., Vol. 105, pp. 17–23, (2000). DOI: 10.1016/S0924-0136(00)00584-7.

[14]. N. T. Hung et al., "*Research on the microstructure and mechanical properties of high-entropy alloys manufactured using 3D printing technology*", J. Mil. Sci. Technol., Vol. 98, pp. 164–170, (2024).

TÓM TẮT

Phân tích thực nghiệm đặc tính dòng bột và đường đơn Inconel 625 trên nền thép SS400 bằng công nghệ bồi đắp kim loại trực tiếp bằng laser

Công nghệ bồi đắp kim loại trực tiếp bằng laser (DLMD) có tiềm năng lớn trong chế tạo lớp phủ và chi tiết hiệu suất cao. Tuy nhiên, ảnh hưởng của tốc độ cấp bột đến độ ổn định dòng bột đồng trục và mối tương quan với chất lượng đường đơn vẫn chưa được nghiên cứu một cách hệ thống. Nghiên cứu khảo sát đặc trưng dòng bột Inconel 625 bằng kỹ thuật chụp ảnh mặt cắt kết hợp phân tích cường độ xám ở tốc độ cấp bột 5–30 g/phút. Dòng bột luôn hội tụ ở khoảng 9 mm dưới miệng phun, không phụ thuộc tốc độ cấp bột, bảo đảm sự đồng trục với chùm laser mà không cần điều chỉnh khoảng cách đầu phun đến bề mặt nền. Các mặt cắt ngang của dòng bột có phân bố dạng Gauss. Dựa trên các kết quả này, bồi đắp đường đơn trên thép SS400 cho hình dạng ổn định, cấu trúc dendrite tế bào - cột mảnh (PDAS 2,2–2,3 µm), độ cứng tế vi 206,7–209,5 HV (cao hơn khoảng 25% so với nền), không xuất hiện rỗ khí, thiếu nóng chảy hoặc nứt đông đặc. Các kết quả này thiết lập mối liên hệ trực tiếp giữa đặc trưng dòng bột và chất lượng bồi đắp, đồng thời cung cấp cơ sở cho quy trình DLMD ổn định đối với Inconel 625 trên nền thép carbon.

Từ khoá: Bồi đắp kim loại trực tiếp bằng laser; Inconel 625; Đặc trưng dòng bột; Đầu phun đồng trục; Đường đơn; Cấu trúc và độ cứng tế vi.